Computer Science Department of The University of Auckland
CITR at Tamaki Campus (http://www.citr.auckland.ac.nz/)

CITR-TR-117 Sep 2002

Recovery of Coloured Surface Reflectances Using the Photometric Stereo Method

Chia-Yen Chen, Reinhard Klette [1]
Ramakrishna Kakarala [2]
and Chi-Fa Chen [3]

Abstract

We discuss a fast and efficient method to estimate the surface reflectance values with respect to different wavelength of light. Qualitative and quantitative evaluations show that surfaces rendered using surface reflectances obtained by the proposed method are more realistic when compared with conventional rendering methods.

1 Centre for Image Technology and Robotics, Tamaki Campus, Building 731, The University of Auckland, Morrin Road, Glen Innes, Auckland 1005, New Zealand.

2 Semiconductor Products Group, Agilent Technologies, Santa Clara CA 95054 USA.

3 Department of Electrical Engineering, I-Shou Univeristy, Kaohsiung, Taiwan

Recovery of Coloured Surface Reflectances Using the Photometric Stereo Method

Chia-Yen Chen, Reinhard Klette, *
Ramakrishna Kakarala †
and
Chi-Fa Chen ‡

Abstract

We discuss a fast and efficient method to estimate the surface reflectance values with respect to different colour channels. Qualitative and quantitative evaluations show that surfaces rendered using surface reflectances obtained by the proposed method are more realistic when compared with conventional rendering methods.

1 Introduction

In previous work [1] we have investigated the estimation of surface reflectance for gray level images. It has been shown that surfaces rendered using calculated reflectance values have more realistic appearances when compared with surfaces rendered using constant reflectance values. The recovered surface reflectance values enable the surface to be rendered realistically under different viewing and illumination conditions. The promising results obtained for gray level images have provided the incentive to investigate the recovery of surface reflectances using colour images. That is, obtaining surface reflectance values with respect to the different wavelengths of light. While it is possible to use spectral mesasuring devices for reflectance measurement, such devices are expensive and require skilled manipulations. In this work, we propose an alternative approach to the estimation of surface reflectance values with respect to different colours, and show that the obtained colour reflectance values are able to produce realistically rendered images. The method that we propose makes use of the albedo independent photometric stereo approach [2, 3, 7, 10]. Photometric stereo is firstly applied to recover the surface normals. The calculated surface normals are then used to extract the reflectance values from the input colour images of the object.

*CITR, Tamaki Campus The University of Auckland, Auckland, New Zealand

†Semiconductor Products Group, Agilent Technologies, Santa Clara CA 95054 USA.

‡Department of Electrical Engineering, I-Shou Univeristy, Kaohsiung, Taiwan

Subjective comparisons show that the surfaces rendered using calculated reflectance values appear more realistic to the viewers. Quantitative comparisons show that intensity values in images rendered using calculated reflectance values are closer to the intensity values in original images than intensity values rendered by the conventional texture mapping approach.

2 Model

The light reflected by a point on a given surface is dependent upon the surface's spectral, geometric and surface factors [6]. The spectral factor describes the colours and distributions of the surface and the illuminant. The geometric factor describes the geometry of viewing and illumination directions with respect to the surface. The surface factor describes the smoothness of the surface material.

The reflectance for each point $\mathbf{t}$ on a surface is given by a wavelength-dependent bidirectional reflectance distribution function (BRDF). The BRDF is defined to be the ratio of reflected radiance to the incident irradiance. At the point $\mathbf{t}$, the BRDF is a function of the incident light direction $\mathbf{s}$, the surface normal $\mathbf{n}$), the direction of view $\mathbf{v}$, and the wavelength λ:

$$BRDF = F_{BRD,\mathbf{t}}(\mathbf{s}, \mathbf{n}, \mathbf{v}, \lambda). \tag{1}$$

Given a 3-D surface, we can calculate the surface normal $\mathbf{n}$ for every point $\mathbf{t}$ on the surface. Assume that we can also determine the illumination direction $\mathbf{s}$ and direction of view $\mathbf{v}$ by calibration. Then it is only necessary to determine how $F_{BRD,\mathbf{t}}$ varies with respect to λ. That is, how the surface reflects incoming light of various wavelengths. The reflectance function is given with respect to λ and represented as $\rho(\lambda)$. The function $\rho(\lambda)$ may be modelled by a low-order orthogonal basis expansion, i.e.,

$$\rho(\lambda) = \sum_{k=1}^{n} \alpha_k x_k(\lambda), \tag{2}$$

and basis functions $x_k(\lambda)$ are determined in [8]. However, in the following we will not use any expansion (i.e. just use $n = 1$). $\rho(\lambda)$ is simply denoted by ρ, because we calculate ρ where λ remains unspecified. At the current stage, we are not yet able to measure with respect to λ and use colour channels to define intervals of λ values.

3 Calculation of surface reflectance values

In the following, we assume the Lambertian reflectance model. The Lambertian reflectance function R for a surface Z under orthographic projection can be written as

$$\begin{aligned} R_j(p,q) &= E_{0_j}\rho_j \, cos\theta_i + \sigma_j \\ &= \eta_j \, cos\theta_i + \sigma_j \end{aligned} \tag{3}$$

where $j = 1, 2, 3$ respectively denotes the three different colour channels, red, green and blue, $p = \partial Z/\partial X$ and $q = \partial Z/\partial Y$ are partial derivatives of the surface Z, η is the composite albedo which combines the light source intensity E_0 and the intrinsic reflectance of surface material ρ, θ_i is the incident angle between the surface normal and light direction, and σ is the bias intensity due to background illumination, sensor calibration and quantization of irradiance values [9]. The bias intensity is assumed to be zero, such that the irradiance equation for the image intensity, E_j, at position (x, y) is expressed as

$$E_j(x,y) = E_{0_j}\rho_j \, cos\theta_i \, . \tag{4}$$

In this work, the photometric stereo method is used to recover the partial surface derivatives p and q, respectively in x and y directions. Since the surface albedo values are initially unknown, an albedo independent approach, derived from Eq. 4, is employed to estimate the local surface orientations [3].

The local surface normals are calculated according to

$$\begin{aligned} \mathbf{u} = (&E_{01}E_2|s_2|s_1 - E_{02}E_1|s_1|s_2) \times \\ &(E_{01}E_3|s_3|s_1 - E_{03}E_1|s_1|s_3), \end{aligned} \tag{5}$$

where $\mathbf{u}$ is a vector collinear to the surface normal $\mathbf{n}$, E_{0i} are the light source intensities, E_i are the image irradiance values and s_i are the light source directions.

Note that it is possible to use other surface recovery methods (such as structured lighting) to obtain the surface depth values, and then differentiate to obtain the partial derivatives p and q.

The calculated surface normals are substituted into the reflectance function to find the composite albedo η_j using an original input image with calibrated light source direction. The value of η_j at position (x, y) is given by

$$\eta_{jk}(x,y) = E_{kj}(x,y)/cos\theta_i \tag{6}$$

where $k = 1, 2..n$ indexes the set of input colour images, and $E_{kj}(x, y)$ denotes the image intensity for the j^{th} channel, at position (x, y) from the k^{th} input image.

Under the ideal assumption of parallel illumination, the incident light has constant direction and surface points with $\theta_i > \pi/2$ will not be illuminated. However, in experimental conditions with a point light source, the scattering of illumination from the light source and the interreflections from the surface both contribute to additional illuminations. The combined effect is such that even regions with $\theta_i > \pi/2$ are illuminated, i.e. self-shadowing of the surface does not occur strictly at the $\theta_i = \pi/2$ boundary. For regions where $cos\,\theta_i < 0$, i.e. the incident angle is in the range of $(-\pi, -\pi/2)$ or $(\pi/2, \pi)$, $cos\,\theta_i$ becomes negative. The reflectance values at positions with negative $cos\,\theta_i$ values are set to 0.

For points where the surface normals are almost perpendicular to the light source direction, values of $cos\,\theta_i$ are close to 0, and the calculated η_j is more likely to be erroneous. Hence values from such points are also eliminated by a threshold operation. The threshold can be determined independently for each situation by setting it to, say the top five percentile of all the calculated η_j values. Values that are larger than the threshold are discarded and remaining η_j values provide an estimation of the surface's reflectivity.

Calculations of the surface reflectance values are performed separately for different colour channels. The calculated surface reflectance values for all three channels on the surface are combined to render colour images given an incident illumination direction.

4 Results

This section show the resultant surface reflectance values calculated according to previously described steps and perform comparisons to determine the effectiveness of the proposed method. The reported results represent progress compared to [1].

Figure 1 shows a set of example input images of a human face. In this set of images, the light source directions are respectively $s_1 = (0.44, 0.28, -1)$, $s_2 = (0.04, -0.16, -1)$, and $s_3 = (-0.36, 0.11, -1)$, from left to right, determined based on inverse photometric stereo method [3].

Figures 2a, 2b and 2c show the distributions of η_j (albedo) values respectively calculated from the colour images with incident illumination directions s_1, s_2 and s_3. In each of the images, the horizontal axis represents the range of η_j values and the vertical axis represents the number of

Figure 1. Examples of input images.

occurrences. Figures 3a, 3b, and 3c show the distributions of the reflectance values for different colour channels calculated from incident illumination respectively at s_1, s_2 and s_3. In Fig. 3a, the left-most picture shows the reflectance distribution of the red channel, the middle picture shows the distribution for the green channel, and the right picture is for the blue channel.

It can be seen from the graphs that irrespective of the incident illumination directions, the calculated surface reflectance values have similar frequency distributions. Furthermore, the distributions of calculated η_j values are also consistent in the spatial domain, as shown in Fig. 3. This observation has been anticipated, since the reflectance function describes the surface's reflectance properties, and should remain constant irrespective of the illumination conditions.

The calculated η_j maps are combined with previously acquired surface depth values to render images from different incident illumination directions. For comparison, we also render a surface which is texture mapped with one of the original input images. Both types of rendered images are compared with an image of the actual surface with the incident illumination direction identical to that of the rendered images.

In the following example, we take the η_j maps acquired with incident illumination direction s_2 as the reflectance map for the face depth data. The reason for using η_j maps with illumination direction s_2 is because we expected s_2 to provide better illumination in terms of coverage (less shadowed regions) and uniformity (various regions on the surface are similarly illuminated). Image regions where shadow and high light values saturate the working range of the camera sensors are likely to cause errorneous results, since the values are no longer mapped linearly. We have also selected the original image acquired with incident illumination direction s_2 to texture map the surface for comparison. The reasons for selecting the texture map are the same as for the reflectance map. Since we will also be rendering the surface with respect to different illumination directions, an image that has the most even illumination is preferable to an image with strong shadows and high lights.

Figure 4 shows the original and rendered RGB images and Fig. 5 shows the Y-component of the original and rendered images. From Figs. 4 and 5, it can be seen that the surface rendered using calculated reflectance values has a closer resemblance to the original images. The reflectance rendered surfaces also appear more realistic than conventional graphics rendering approaches for human skin. Tex-

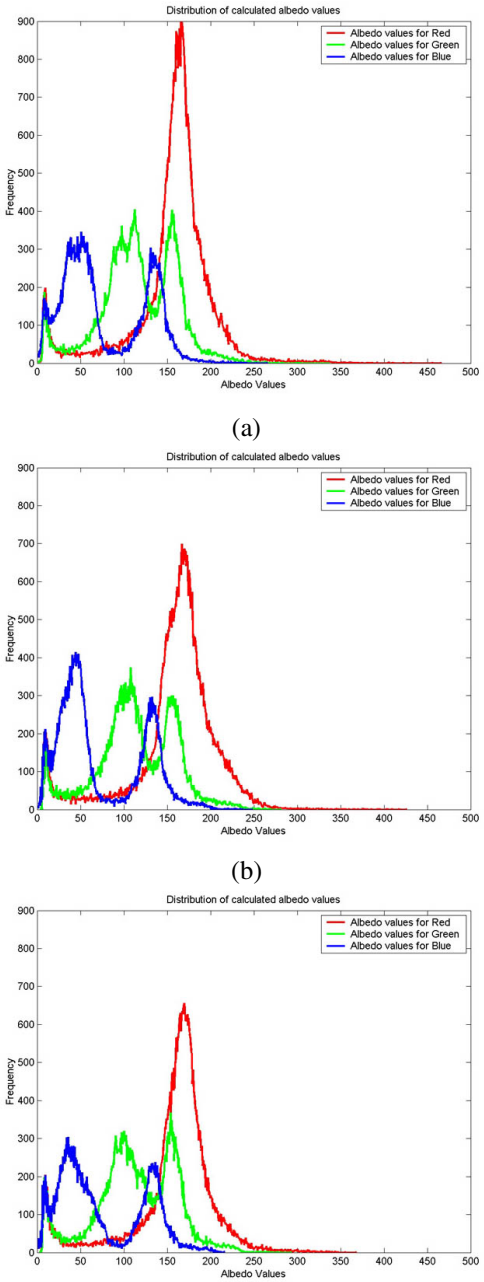

Figure 2. Frequency distribution of calculated η_j values for (a) s_1, (b) s_2, and (c) s_3.

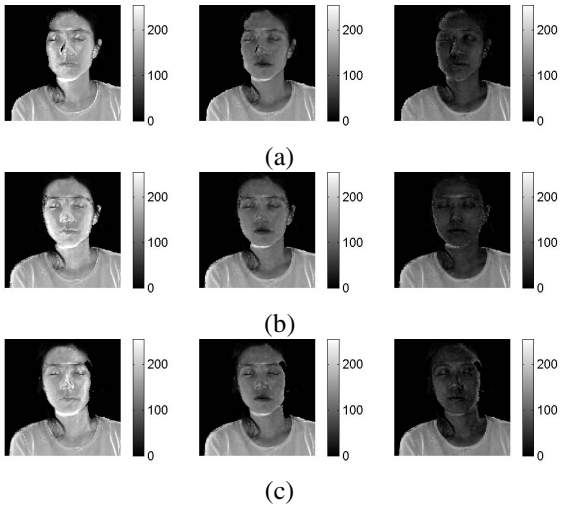

Figure 3. Spatial distribution of calculated η_j values for (a) s_1, (b) s_2, and (c) s_3.

ture mapped surfaces on the other hand, are more susceptible to error when the illumination given for rendering contradicts with the incident illumination direction of the texture map used. Errors in the resultant reflectance maps are perceptible in the rendered images for regions of the input image where shadows occur. Nevertheless, for most regions, in particular regions with smaller changes in the colour and surface gradients, are rendered quite convincingly.

Quantitatively, the images rendered with reflectance maps calculated using the proposed method have lower error values compared to the surface rendered with texture map. Tables 1 and 2 show the mean square error between the original images and images rendered using reflectance maps calculated using the proposed method.

s_1	e_R $(\times 10^{-4})$	e_G $(\times 10^{-4})$	e_B $(\times 10^{-4})$
Reflectance (s_2)	8.9	1.8	4.5
Reflectance (s_3)	44.2	13.1	9.6
Texture (s_2)	89.3	47.4	22.4
s_3	e_R $(\times 10^{-4})$	e_G $(\times 10^{-4})$	e_B $(\times 10^{-4})$
Reflectance (s_1)	60.1	28.3	22.9
Reflectance (s_2)	8.9	2.6	4.6
Texture (s_2)	11.7	61.7	31.1

Table 1. MSE in RGB channels of reflectance and texture rendered images for s_1 and s_3.

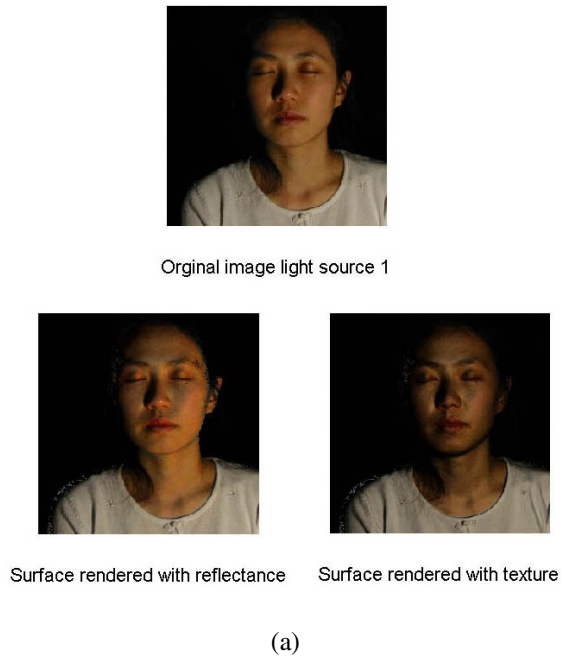

Figure 4. Original, reflectance rendered, and texture map rendered images of the surface for (a)s_1 and (b)s_3.

Each half of Table 1 shows the MSE in each colour channel (e_R, e_G, e_B) for a surface rendered using reflectance maps obtained from input images, or rendered using a tex-

ture map. For example, in the top half of Table 1, the incident light direction for rendering in s_1. In the column for red channel (e_R), the MSE for a surface rendered with reflectance map calculated from incident light direction s_2 is 8.9×10^{-4}, for a surface rendered with reflectance map calculated from incident light direction s_3 is 44.2×10^{-4}, and for a surface rendered using a texture map illuminated from s_2 is 89.3×10^{-4}.

Overall, it can be seen from Table 1 that the differences between images rendered using calculated reflectance maps are significantly smaller than that between images rendered using a texture mapped surface. In fact, for the reflectance map calculated from our selected incident illumination direction s_2, the errors are often less than that of the texture mapped surface by more than a factor of 10. Errors in image rendered using reflectance map from incident illumination of s_3 are also smaller than texture mapped images. Same results can be observed in the lower half of the table where the rendered incident illumination direction is s_3.

The MSE in the YIQ channels (e_Y, e_I, e_Q) of the rendered and original images has also been calculated to show the performance of rendering using reflectance maps with respect to the YIQ components. Table 2 shows the MSE in the YIQ component for the resultant rendered images. In conjunction with Fig. 5, we can see that in the Y-channel, the surface rendered with calculated reflectance maps have higher correspondence to the original images than surface rendered with texture mapping. The magnitude of improvement is quantised by the values in Table 2. As observed before, the error in images rendered using reflectance map is significantly smaller than texture mapped images.

From above results, it can be seen that the input image with incident illumination direction s_2 provide the best results. This is in agreement with the expectation that the input image most suitable for reflectance recovery should have the surface as fully and as uniformly illuminated as possible. Nevertheless, reflectances recovered from less ideally illuminated surfaces are still able to yield reasonable rendering results.

s_1	e_Y $(\times 10^{-4})$	e_I $(\times 10^{-4})$	e_Q $(\times 10^{-4})$
Reflectance (s_2)	1.6	5.2	0.3
Reflectance (s_3)	15.6	13.1	0.5
Texture (s_2)	53.2	5.4	2.7
s_3	e_Y $(\times 10^{-4})$	e_I $(\times 10^{-4})$	e_Q $(\times 10^{-4})$
Reflectance (s_1)	30.6	13.4	0.6
Reflectance (s_2)	2.4	4.6	0.3
Texture (s_2)	69.9	10.5	0.3

Table 2. MSE in YIQ channels of reflectance and texture rendered images for s_1 and s_3.

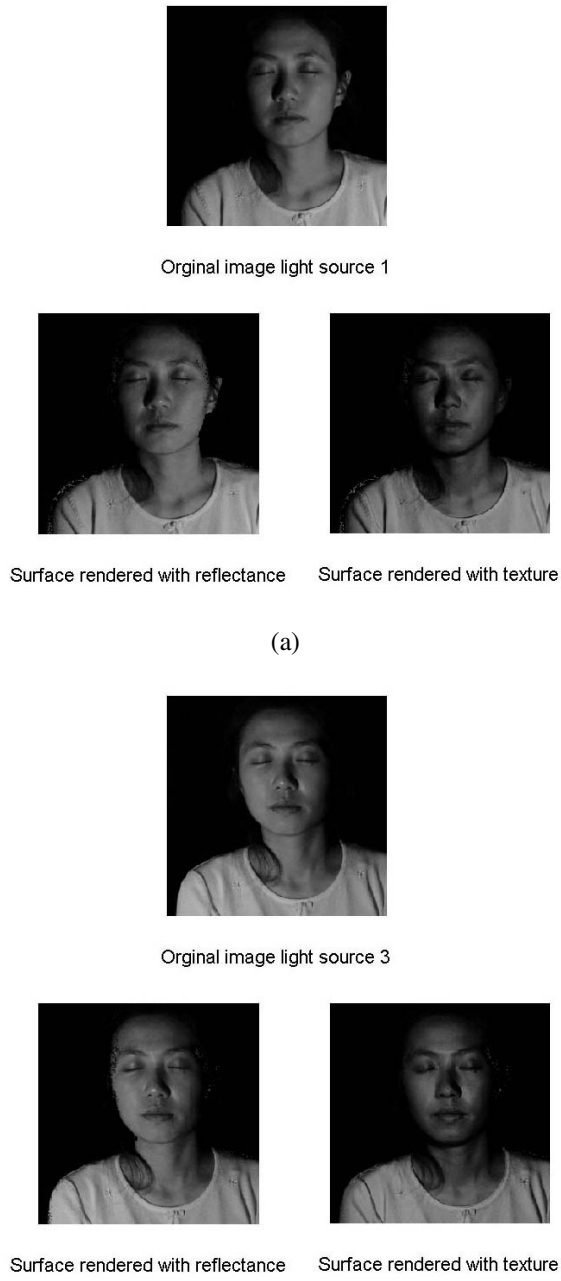

Figure 5. Original, reflectance rendered, and texture map rendered luminance images of the surface for (a)s_1 and (b)s_3.

In this work, errors in the rendered images are mainly due to the inaccuracy in the surface values of the recovered surface and saturation of the camera sensors in shadow and highlight regions. Such factors cause the albedo values to be incorrectly recovered, resulting in the colour variations observed in the rendered images. In real situations, factors such as interreflection, sensor calibration and the spread of illumination will also affect the perceived surface reflectance values. Hence, in future work, we will need to take the bias intensity, σ, into consideration while performing surface reflectance calculations, to improve the result of calculated reflectance values.

5 Conclusions

In this work, we have proposed a method to estimate the surface reflectance function with respect to different colour channels. The proposed method is used in conjunction with the photometric stereo method to recover the specific surface reflectance map for a particular surface. Note that a measurement of the light source intensity E_0 would allow the derivateion of ρ from η.

Overall, it has been shown that the proposed method provides a simple and effective approach to recover the surface reflectance function with respect to each point on the visible surface. If the surface reflectance matches the Lambertian assumption, images rendered using the calculated reflectance map also appear more realistic, and have values closer to the original surface than images rendered using texture map. The surface reflectance function can be mapped onto the 3D surface of the object to render convincing visualisations from different lighting and viewing conditions. In future work, we will further evaluate the proposed method by applying it to a larger data set of colour images and surfaces.

References

[1] C. Chen, R. Klette and R. Kakarala: Albedo recovery using a photometric stereo approach, *Proc. of ICPR*, Vol. 3, 2002, pp. 700-703.

[2] R. Klette, K.Schlüns: Height data from gradient fields, *Proc. of SPIE*, 2908, 1996, pp. 204-215.

[3] R. Klette, K. Schlüns and A. Koschan: *Computer Vision: Three-dimensional Data from Images*. Springer, Singapore, 1998 (German version, 1996).

[4] R. Klette, R. Kozera and K. Schlüns,: Shape from shading and photometric stereo methods, *Handbook of Computer Vision and Applications*, Vol. 2, Academic Press, San Diego, 1999, pp. 531-590.

[5] Y. Murakami, T. Obi, M. Yamaguchi, N. Ohyama and Y. Komiya: Spectral reflectance estimation from multi-band image using color chart, *Optics Communication*, Vol. 188, 2001, pp. 47-54.

[6] S. Tominaga and N. Tanaka: Estimating reflection parameters from a single color image, *IEEE Computer Graphics and Applications*, Vol. 20, 2000, pp. 28-66.

[7] R. J. Woodham: Photometric method for determining surface orientation from multiple images, *Optical Engineering*, Vol. 19, 1980, pp. 139-144.

[8] M. J. Vrhel, R. Gershon and L. S. Iwan: Measurement and analysis of object reflectance spectra, *Color Research and Application*, Vol. 19, 1994, pp. 4-9.

[9] Q. Zheng and R. Chellappa: Estimation of illuminant direction, albedo, and shape from shading, *IEEE Transaction on Pattern Analysis and Machine Intelligence*, Vol. 13, 1991, pp. 680-702.

[10] R. Zhang, P. S. Tsai, J. E. Cryer and M. Shah: Shape-from-shading: a survey, *IEEE Transaction on Pattern Analysis and Machine Intelligence*, Vol. 21, 1999, pp. 690-706.